Journal of Control, Automation and Electrical Systems (2020) 31:447–460
https://doi.org/10.1007/s40313-019-00546-y

Robust Model Predictive Controller Applied to Three-Phase Grid-Connected LCL Filters

L. A. Maccari Jr.[1] · D. M. Lima[1] · G. G. Koch[2] · V. F. Montagner[2]

Received: 10 August 2019 / Revised: 16 October 2019 / Accepted: 7 November 2019 / Published online: 21 November 2019

Abstract
Grid-connected inverters play an important role in renewable energy system nowadays, serving as an interface between the renewable energy source and the grid. However, the PWM modulation used to control the converters produces harmonic content that must be filtered properly. In this paper, an active damping strategy is used with a three-phase power converter with an LCL filter to achieve harmonic rejection. The control strategy which will be used is a continuous control set model predictive control (CCS-MPC) based on a state-space model of the system. This controller must ensure that the injected grid currents track sinusoidal references and reject harmonic disturbances from the grid voltage. This is achieved by using an augmented model of the system that contains resonant controllers. Following the unconstrained CCS-MPC methodology, a fixed gain controller that can be implemented similarly to a classical state-space feedback controller is obtained. An analysis of the impact of the CCS-MPC tuning parameters on the closed-loop response is made. Also, an *a posteriori* linear matrix inequality approach is used to show that the resulting closed-loop system is robust in regard to grid inductance uncertainties and variations. Simulation and experimental test results show that the proposed controller yields good results, complying with the IEEE 1547 Standard grid currents harmonic limits.

Keywords Model predictive control · LCL filter · Grid-connected converters · Current control · LMI robust analysis

1 Introduction

An important engineering problem with renewable energy systems is the connection with the electric grid. The interface between the primary renewable energy source and the grid is usually carried out by a power converter which is responsible for the power control of the system. Generally, low-pass filters are used in order to reduce the harmonic content of the currents injected into the grid, which are caused by the PWM modulation. The limits for this harmonic content are determined by international standards such as IEEE 1547, IEC 61727 or IEC 61000-3-2 standards (IEEE 2011; IEC 2004, 2018).

The most used filter topology is the LCL filter. It is chosen for its attenuation (−60 dB/decade) and size of reactive elements, which are smaller than an L filter for the same power (Teodorescu et al. 2011). The main drawback of LCL filters is the presence of a resonance peak that can lead the system to a poor performance or even to instability. Many solutions were studied to cope with this resonance peak, and they can be divided in passive and active damping strategies. Passive damping strategies deal with the addition of passive elements, usually resistances, to the filter. However, this can increase the power losses and reduce the system efficiency (Peña-Alzola et al. 2013). On the other hand, active damping strategies can cope with the resonance peak without the addition of new elements only by adding a suitable control strategy, thus being preferred because they do not need any hardware modifications and do not increase the conduction losses.

✉ D. M. Lima
daniel.lima@ufsc.br

L. A. Maccari Jr.
luizmaccari@gmail.com

G. G. Koch
gustavoguilhermekoch@gmail.com

V. F. Montagner
vfmontagner@gmail.com

[1] Universidade Federal de Santa Catarina, Rua João Pessoa no 2514, Blumenau, Santa Catarina CEP: 89036-256, Brazil

[2] Universidade Federal de Santa Maria, Av. Roraima no 1000, Santa Maria, Rio Grande do Sul CEP: 97105-900, Brazil

The main control objectives for grid-connected inverters are: reference tracking of sinusoidal references, which is responsible for the control of active and reactive power; disturbance rejection of grid voltages, which is necessary to comply with grid standards; robustness against uncertain grid impedances, since the grid characteristics are not the same for different connection points; and resonance peak damping. To achieve these objectives, many strategies can be used; the main ones are the proportional plus resonant (PR) controller and the synchronous reference frame proportional integral (SRFPI) controller. PR controllers are designed on the stationary reference frame and use multiple resonant controllers to ensure the reference tracking and disturbance rejection of a specific harmonic content. To deal with the active damping, they use an auxiliary filter, commonly a notch filter. The main problem with these approaches is the difficulty associated with tuning multiple resonant controllers because of the narrow stability margins (Twining and Holmes 2003).

The most used control technique is the SRFPI controller, which is designed in a synchronous reference frame using the dq-transformation, changing the problem of tracking a sinusoidal reference for a regulation one. Its major drawback is that, unlike the case of L filters, the d and q coordinates for LCL filters are not completely decoupled which can reduce the performance during transients. Another important issue to be addressed is that when multiple harmonics have to be rejected, it has to use multiple reference frames, which increases the implementation complexity (Liserre et al. 2006).

Another alternative which achieved good results are time-domain strategies. Control systems with gains designed by the linear quadratic regulator (LQR) method are presented in Wu and Lehn (2006), Huerta et al. (2012), Kukkola and Hinkkanen (2013) and Busada et al. (2015). This technique has as the main characteristic the avoidance of the problem of selecting specific pole locations with a procedure that always ensures stable control gains and good stability margins (Safonov and Athans 1977).

Another important characteristic of grid-connected applications is the uncertainty on the grid impedance which leads to the study of control techniques that ensures stability and performance for systems with parametric uncertainties and variations. For example, the works (Maccari et al. 2014, 2015, 2017) and Koch et al. (2019) deal with linear matrix inequalities (LMI) control techniques to design control gains which provide good results even under parametric uncertainties and variations. The approach used in these papers includes resonant controllers in the filter model providing an unified control design method able to track sinusoidal references and reject harmonic disturbances.

Among time-domain techniques, the model predictive control (MPC) is one of the most known, being largely used for many practical applications. This type of controller became very popular in several industrial applications since the late 1970s (Qin and Badgwell 2003; Camacho and Bordons 2004). However, their use for power electronics is relatively recent (Sultana et al. 2017; Rodriguez et al. 2013) being an important topic for researchers in recent years (Panten et al. 2016; Nauman and Hasan 2016; Young et al. 2016). The use of MPC controllers for power converters can be divided in two sections: finite control set controllers (FCS-MPC) and continuous control set controllers (CCS-MPC) (Falkowski and Sikorski 2018b; Vazquez et al. 2017).

The FCS-MPC consists in the use of an MPC algorithm with a control law which assumes only a specified set of values (Kouro et al. 2009). This type of controller leads to a nonlinear control law calculated at every sample period. The control law gives the state signals to the switches of the inverter directly, substituting the traditional space vector modulation (SVM), resulting in a variable switching frequency pattern. This technique allows to obtain controllers with good transient responses, low switching frequencies and good reference tracking. It has been used recently in power electronics systems, for example, in active power filters (Ferreira et al. 2018), in grid-connected inverters (Falkowski and Sikorski 2018a, b), and in the power control of grid-connected photovoltaic panels (Lekouaghet et al. 2018). In spite of the good results, the main drawback of the FCS-MPC is the nonlinearity of the controller, which does not allow the use of any linear analysis technique to study the robustness of the system. Moreover, when constraints are inserted to achieve robust performance and stability against parametric uncertainties and variations, the MPC has a high computational burden, which may be a restriction considering the limitations imposed by the sampling frequency (Camacho and Bordons 2004). Another important drawback is the fact of that the variable switching frequency can cause some problems such as acoustic noise, vibration and electrical resonances (Kouro et al. 2009).

Taking into account the limitations of the FCS-MPC controller, this paper has as main contribution the use of an unconstrained robust CCS-MPC controller for the current control of three-phase grid-connected inverters with LCL filters under uncertainties of the grid inductances. The CCS-MPC provides an MPC controller with fixed gains, which can be implemented as a traditional full state-feedback control law using a classical SVM. This approach is easier to implement than an FCS-MPC controller as it uses the same control structure of other state-space controllers, with low computational costs, and the fixed switching frequency does not spread the harmonic content along the frequency spectrum (Kouro et al. 2009).

Moreover, since the resulting controller is linear, classical linear analysis tools can be used, such as, for example, closed-loop frequency responses. Here, to study and to ensure the robustness of the closed-loop system under grid inductance

variations, an *a posteriori* LMI robust stability analysis is carried out. This strategy results in a robust MPC controller without using constraints in the optimization algorithm, reducing the control burden and providing a linear state-space controller (Rodriguez et al. 2013).

The main control objectives accomplished by the controller proposed here are: (1) robust performance under parametric uncertainties; (2) stability against parametric variations; (3) grid disturbance rejection of specific harmonic content; (4) tracking of sinusoidal references and (5) compliance with the limits for current harmonics injected into the grid presented in the IEEE 1547 standard, the most important grid regulation code. All these control objectives can be achieved by an unconstrained MPC controller with fixed gains using the same control structure as other state-space approaches. The results presented in this paper expand the ones in Maccari et al. (2016) by applying the MPC controller to a three-phase system, instead of a single-phase one, by doing the study of the impact of different control parameters on the system performance, by adding a robustness analysis using LMIs and by adding experimental results which complies with harmonic limits described in IEEE 1547 Standard.

The paper is organized as follows: the model of the plant is presented in Sect. 2; the MPC controller is described in Sect. 3; in Sect. 4, a robust stability analysis of the closed-loop system based on LMIs is performed; in Sect. 5, simulation and experimental results are shown, and, finally, in Sect. 6 the conclusions are presented.

2 System Model

Consider the circuit depicted in Fig. 1. The LCL filter represents the plant, whose control inputs are given by the voltages of the three-phase inverter, the outputs are the currents injected into the grid, and the disturbance inputs are given by the grid voltages, which can also include harmonics. The states considered here are the currents of the converter-side inductors, i_{ca}, i_{cb}, i_{cc}, the currents of the grid-side inductors, i_{gc}, i_{gb}, i_{gc} and the capacitor voltages, v_{ca}, v_{cb}, v_{cc}. The control signals which command the inverter switches are generated by a digital signal processor (DSP) by means of a full state-feedback control law. The grid is assumed to be predominantly inductive, being modeled, per phase, by a voltage source in series with an inductance L_{g2}. It is known that the DC bus voltage control and the synchronization with the grid voltage are important issues for grid-connected applications (Bianchi et al. 2012; Umbrí et al. 2014). However, in the current paper it is assumed that the DC input voltage is constant and that the synchronization with the voltages at the point of common coupling (PCC) is already given (Cardoso et al. 2008).

In order to obtain a model for the system described in Fig. 1, it is also assumed that the converter uses ideal switches and the switching frequency is much higher than the grid fundamental frequency, allowing, for control design purposes, to neglect the effect of PWM harmonics in the voltages generated by the converter (Teodorescu et al. 2011).

Thus, a state-space representation of the LCL filter can be obtained, generating a model with 9 variables, 3 control inputs and 3 disturbance inputs, represented by

$$\frac{\mathrm{d}\mathbf{x}_{abc}}{\mathrm{dt}} = \mathbf{A}_{abc}\mathbf{x}_{abc} + \mathbf{B}_{uabc}\mathbf{u}_{abc} + \mathbf{B}_{dabc}\mathbf{v}_{dabc} \tag{1}$$

with

$$\mathbf{A}_{abc} = \begin{bmatrix} \mathbf{0}_{3\times3} & \mathbf{A}_{p1} & \mathbf{0}_{3\times3} \\ \mathbf{A}_{p2} & \mathbf{0}_{3\times3} & -\mathbf{A}_{p2} \\ \mathbf{0}_{3\times3} & \mathbf{A}_{p3} & \mathbf{0}_{3\times3} \end{bmatrix},$$

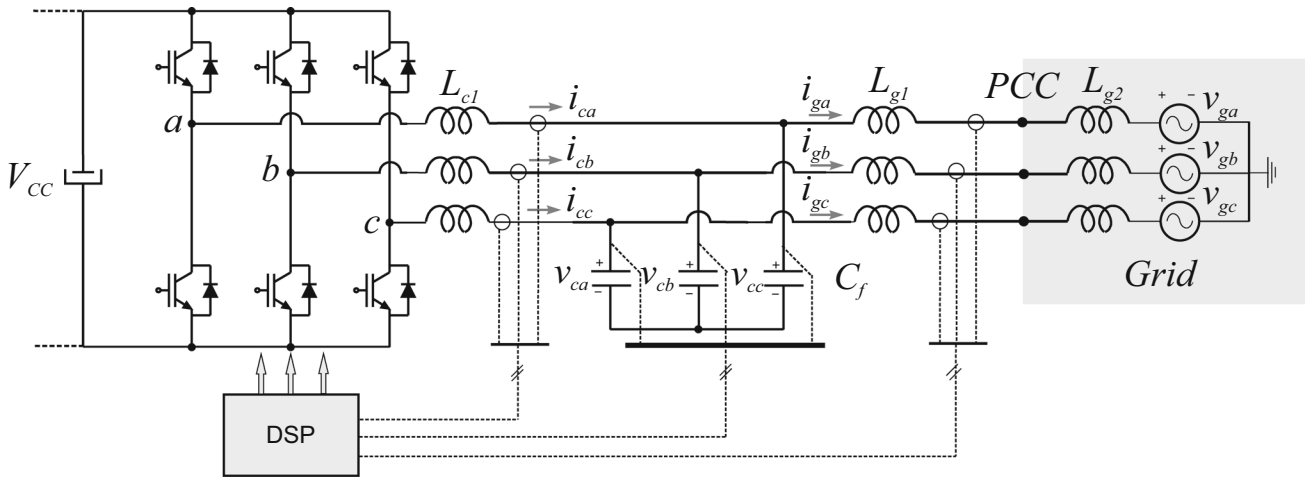

Fig. 1 Three-phase inverter connected to the grid with of an LCL filter (Maccari et al. 2017)

$$\mathbf{B}_{uabc} = \begin{bmatrix} -\mathbf{A}_{p1} \\ \mathbf{0}_{3\times3} \\ \mathbf{0}_{3\times3} \end{bmatrix}, \mathbf{B}_{dabc} = \begin{bmatrix} \mathbf{0}_{3\times3} \\ \mathbf{0}_{3\times3} \\ -\mathbf{A}_{p3} \end{bmatrix} \tag{2}$$

and with

$$\mathbf{A}_{p1} = \begin{bmatrix} -\frac{2}{3L_{c1}} & \frac{1}{3L_{c1}} & \frac{1}{3L_{c1}} \\ \frac{1}{3L_{c1}} & -\frac{2}{3L_{c1}} & \frac{1}{3L_{c1}} \\ \frac{1}{3L_{c1}} & \frac{1}{3L_{c1}} & -\frac{2}{3L_{c1}} \end{bmatrix},$$

$$\mathbf{A}_{p2} = \begin{bmatrix} \frac{1}{C_f} & 0 & 0 \\ 0 & \frac{1}{C_f} & 0 \\ 0 & 0 & \frac{1}{C_f} \end{bmatrix},$$

$$\mathbf{A}_{p3} = \begin{bmatrix} \frac{2}{3L_g} & -\frac{1}{3L_g} & -\frac{1}{3L_g} \\ -\frac{1}{3L_g} & \frac{2}{3L_g} & -\frac{1}{3L_g} \\ -\frac{1}{3L_g} & -\frac{1}{3L_g} & \frac{2}{3L_g} \end{bmatrix} \tag{3}$$

where L_{c1}, C_f, and L_{g1} are, respectively, the converter-side inductance, the filter capacitance, and the grid-side inductance. Also,

$$L_g = L_{g1} + L_{g2} \tag{4}$$

The state vector $\mathbf{x}_{abc}$, the input vector $\mathbf{u}_{abc}$ and the disturbances vector $\mathbf{v}_{dabc}$ are given as follows:

$$\mathbf{x}_{abc} = \begin{bmatrix} i_{ca} \\ i_{cb} \\ i_{cc} \\ v_{ca} \\ v_{cb} \\ v_{cc} \\ i_{ga} \\ i_{gb} \\ i_{gc} \end{bmatrix}, \quad \mathbf{u}_{abc} = \begin{bmatrix} u_a \\ u_b \\ u_c \end{bmatrix}, \quad \mathbf{v}_{dabc} = \begin{bmatrix} v_{ga} \\ v_{gb} \\ v_{gc} \end{bmatrix} \tag{5}$$

To avoid the problem of coupling between phases, the three-phase system can be reduced to a decoupled two-phase system by means of the well known transformation of abc coordinates to $\alpha\beta0$ coordinates, whose transformation matrix is given by Duesterhoeft et al. (1951)

$$\mathbf{T}_{\alpha\beta0} = \frac{2}{3}\begin{bmatrix} 1 & -\frac{1}{2} & -\frac{1}{2} \\ 0 & \frac{\sqrt{3}}{2} & -\frac{\sqrt{3}}{2} \\ \frac{1}{2} & \frac{1}{2} & \frac{1}{2} \end{bmatrix} \tag{6}$$

The change of coordinates is addressed by the multiplication of the vectors $\mathbf{u}_{abc}$ and $\mathbf{v}_{dabc}$ by the matrix $\mathbf{T}_{\alpha\beta0}$ and by the multiplication of the vector $\mathbf{x}_{abc}$ by the matrix

$$\mathbf{T}_a = \begin{bmatrix} \mathbf{T}_{\alpha\beta0} & \mathbf{0}_{3\times3} & \mathbf{0}_{3\times3} \\ \mathbf{0}_{3\times3} & \mathbf{T}_{\alpha\beta0} & \mathbf{0}_{3\times3} \\ \mathbf{0}_{3\times3} & \mathbf{0}_{3\times3} & \mathbf{T}_{\alpha\beta0} \end{bmatrix} \tag{7}$$

Then, the vectors in $\alpha\beta0$ coordinates are given by

$$\begin{aligned} \mathbf{x}_{\alpha\beta0} &= \mathbf{T}_a \mathbf{x}_{abc} \\ \mathbf{u}_{\alpha\beta0} &= \mathbf{T}_{\alpha\beta0} \mathbf{u}_{abc} \\ \mathbf{v}_{d\alpha\beta0} &= \mathbf{T}_{\alpha\beta0} \mathbf{v}_{dabc} \end{aligned} \tag{8}$$

Using the same reasoning, the system matrices in $\alpha\beta0$ coordinates can be written as

$$\begin{aligned} \mathbf{A}_{\alpha\beta0} &= \mathbf{T}_a^{-1} \mathbf{A}_{abc} \mathbf{T}_a \\ \mathbf{B}_{u\alpha\beta0} &= \mathbf{T}_a^{-1} \mathbf{B}_{uabc} \mathbf{T}_{\alpha\beta0} \\ \mathbf{B}_{d\alpha\beta0} &= \mathbf{T}_a^{-1} \mathbf{B}_{dabc} \mathbf{T}_{\alpha\beta0} \\ \mathbf{C}_{\alpha\beta0} &= \mathbf{C}_{abc} \mathbf{T}_a \end{aligned} \tag{9}$$

and the transformed system is described by

$$\begin{aligned} \dot{\mathbf{x}}_{\alpha\beta0} &= \mathbf{A}_{\alpha\beta0} \mathbf{x}_{\alpha\beta0} + \mathbf{B}_{u\alpha\beta0} \mathbf{u}_{\alpha\beta0} + \mathbf{B}_{d\alpha\beta0} \mathbf{v}_{d\alpha\beta0} \\ y_{\alpha\beta0} &= \mathbf{C}_{\alpha\beta0} \mathbf{x}_{\alpha\beta0} \end{aligned} \tag{10}$$

with the following state, control and disturbance vectors:

$$\begin{aligned} \mathbf{x}'_{\alpha\beta0} &= [i_{c\alpha} \;\; i_{c\beta} \;\; i_{c0} \;\; v_{c\alpha} \;\; v_{c\beta} \;\; v_{c0} \;\; i_{g\alpha} \;\; i_{g\beta} \;\; i_{g0}] \\ \mathbf{u}'_{\alpha\beta0} &= [u_\alpha \;\; u_\beta \;\; u_0] \\ \mathbf{v}'_{d\alpha\beta0} &= [v_{d\alpha} \;\; v_{d\beta} \;\; v_{d0}] \end{aligned} \tag{11}$$

Considering that the system is three-wired, with no path to the current axis '0,' the state-space equations can be reorganized as follows (Duesterhoeft et al. 1951; Teodorescu et al. 2011)

$$\begin{bmatrix} \dot{\mathbf{x}}_\alpha \\ \dot{\mathbf{x}}_\beta \end{bmatrix} = \begin{bmatrix} \mathbf{A} & \mathbf{0} \\ \mathbf{0} & \mathbf{A} \end{bmatrix} \begin{bmatrix} \mathbf{x}_\alpha \\ \mathbf{x}_\beta \end{bmatrix} + \begin{bmatrix} \mathbf{B}_u & \mathbf{0} \\ \mathbf{0} & \mathbf{B}_u \end{bmatrix} \begin{bmatrix} u_\alpha \\ u_\beta \end{bmatrix} + \begin{bmatrix} \mathbf{B}_d & \mathbf{0} \\ \mathbf{0} & \mathbf{B}_d \end{bmatrix} \begin{bmatrix} v_{d\alpha} \\ v_{d\beta} \end{bmatrix} \tag{12}$$

In (12), there are two decoupled systems: one in coordinate α and the other in coordinate β. For controller design purposes, it is possible to consider two decoupled and identical systems: one associated with α-coordinate and another with β-coordinate. Since they are identical, there is need to design only one controller, which is then replicated for the other system. The difference between the control loops will only be in the reference signals.

Omitting the subscripts α and β to simplify notation, the state-space model for control design purposes is given by

$$\dot{\mathbf{x}} = \mathbf{A}\mathbf{x} + \mathbf{B}_u u + \mathbf{B}_d v_d \tag{13}$$

where

$$\mathbf{A} = \begin{bmatrix} 0 & -\frac{1}{L_{c1}} & 0 \\ \frac{1}{Cf} & 0 & -\frac{1}{Cf} \\ 0 & \frac{1}{L_g} & 0 \end{bmatrix}, \ \mathbf{B}_u = \begin{bmatrix} \frac{1}{L_{c1}} \\ 0 \\ 0 \end{bmatrix},$$
$$\mathbf{B}_d = \begin{bmatrix} 0 \\ 0 \\ -\frac{1}{L_g} \end{bmatrix}, \ \mathbf{x} = \begin{bmatrix} i_c \\ v_c \\ i_g \end{bmatrix} \tag{14}$$

The equation of the output is given by

$$y = \mathbf{C}_c\mathbf{x}\,, \ \mathbf{C}_c = [0\ 0\ 1] \tag{15}$$

Since MPC algorithms are inherently discrete, the model must be discretized. Considering a zero-order hold (ZOH) discretization, the following discrete model is obtained from (13)

$$\mathbf{x}(k+1) = \mathbf{G}\mathbf{x}(k) + \mathbf{H}u(k) + \mathbf{H}_d v_d(k) \tag{16}$$

where

$$\mathbf{G} = \mathrm{e}^{\mathbf{A}T_s}, \ \ \mathbf{H} = \mathbf{B}_u \int_0^{T_s} \mathrm{e}^{\mathbf{A}}\mathrm{d}t, \ \ \mathbf{H}_d = \int_0^{T_s} \mathrm{e}^{\mathbf{A}}\mathrm{d}t\mathbf{B}_d \tag{17}$$

Based on the internal model principle (Francis and Wonham 1976), to ensure tracking of a sinusoidal reference and also to ensure rejection of sinusoidal harmonic disturbances, it is necessary to have in the open-loop transfer function poles at $\mathrm{e}^{\pm j w_i T_s}$, where T_s is the sampling period and w_i are the frequencies to be tracked or rejected. Resonant controllers can be used to ensure these properties (Zmood and Holmes 2003). One of these resonant controllers, written in discrete-time state-space equations, can be given by the realization

$$\boldsymbol{\xi}(k+1) = \mathbf{R}\boldsymbol{\xi}(k) + \mathbf{T}e(k) \tag{18}$$

where

$$\mathbf{R} = \begin{bmatrix} a & b \\ 1 & 0 \end{bmatrix}, \ \mathbf{T} = \begin{bmatrix} c \\ 0 \end{bmatrix}$$

and where $e(k)$ is the tracking error, given by

$$e(k) = i_{\mathrm{ref}}(k) - y(k) \tag{19}$$

Assuming the entire state vector $\boldsymbol{\xi}(k)$ as output for the controller (18), the transfer matrix from e to $\boldsymbol{\xi}$ is given by

$$\boldsymbol{\xi}(z) = ((z\mathbf{I} - \mathbf{R})^{-1}\mathbf{T})e(z) = \begin{bmatrix} \frac{cz}{z^2 - az - b} \\ \frac{c}{z^2 - az - b} \end{bmatrix} \tag{20}$$

Notice that the eigenvalues of $\mathbf{R}$ are also the poles of the resonant controllers in (20), since there is no cancellation of zeros and poles. Given a suitable choice of a and b, one has ensured the assignment of the pair of poles of the resonant controllers at $\mathrm{e}^{\pm j w_i T_s}$.

A set of resonant controllers at the frequencies of the fundamental w_o, third, fifth and seventh harmonics ($3w_o$, $5w_o$, $7w_o$) can be written as in (18) with dynamic matrices $\mathbf{R}_1$, $\mathbf{R}_3$, $\mathbf{R}_5$ and $\mathbf{R}_7$, respectively, and with input vectors $\mathbf{T}_1$, $\mathbf{T}_3$, $\mathbf{T}_5$ and $\mathbf{T}_7$, respectively. These harmonics are common in the grid and were chosen to compose the resonant controller in order to ensure good harmonic attenuation (Teodorescu et al. 2011). Also, an additional state representing the one-step delay in control action coming from the digital implementation can be inserted in the model. This leads to an augmented state-space model which has the plant states, the delayed control and the internal states of the resonant controllers, described in detail by (21).

$$\begin{bmatrix} \mathbf{x}(k+1) \\ \phi(k+1) \\ \xi_1(k+1) \\ \xi_2(k+1) \\ \xi_3(k+1) \\ \xi_4(k+1) \\ \xi_5(k+1) \\ \xi_6(k+1) \\ \xi_7(k+1) \\ \xi_8(k+1) \end{bmatrix} = \begin{bmatrix} \mathbf{G}(\boldsymbol{p}) & \mathbf{H}(\boldsymbol{p}) & 0 & 0 & 0 & 0 & 0 & 0 & 0 & 0 \\ \mathbf{0}_{1\times3} & 0 & 0 & 0 & 0 & 0 & 0 & 0 & 0 & 0 \\ -\mathbf{T}_{1(1,1)}\mathbf{C}_c & 0 & \mathbf{R}_1(1,1) & \mathbf{R}_1(1,2) & 0 & 0 & 0 & 0 & 0 & 0 \\ \mathbf{0}_{1\times3} & 0 & 1 & 0 & 0 & 0 & 0 & 0 & 0 & 0 \\ -\mathbf{T}_{3(1,1)}\mathbf{C}_c & 0 & 0 & 0 & \mathbf{R}_3(1,1) & \mathbf{R}_3(1,2) & 0 & 0 & 0 & 0 \\ \mathbf{0}_{1\times3} & 0 & 0 & 0 & 1 & 0 & 0 & 0 & 0 & 0 \\ -\mathbf{T}_{5(1,1)}\mathbf{C}_c & 0 & 0 & 0 & 0 & 0 & \mathbf{R}_5(1,1) & \mathbf{R}_5(1,2) & 0 & 0 \\ \mathbf{0}_{1\times3} & 0 & 0 & 0 & 0 & 0 & 1 & 0 & 0 & 0 \\ -\mathbf{T}_{7(1,1)}\mathbf{C}_c & 0 & 0 & 0 & 0 & 0 & 0 & 0 & \mathbf{R}_7(1,1) & \mathbf{R}_7(1,2) \\ \mathbf{0}_{1\times3} & 0 & 0 & 0 & 0 & 0 & 0 & 0 & 1 & 0 \end{bmatrix} \begin{bmatrix} \mathbf{x}(k) \\ \phi(k) \\ \xi_1(k) \\ \xi_2(k) \\ \xi_3(k) \\ \xi_4(k) \\ \xi_5(k) \\ \xi_6(k) \\ \xi_7(k) \\ \xi_8(k) \end{bmatrix}$$

$$+ \begin{bmatrix} \mathbf{0}_{3\times1} \\ 1 \\ 0 \\ 0 \\ 0 \\ 0 \\ 0 \\ 0 \\ 0 \\ 0 \end{bmatrix} u(k) + \begin{bmatrix} \mathbf{H}_d(\boldsymbol{p}) \\ 0 \\ 0 \\ 0 \\ 0 \\ 0 \\ 0 \\ 0 \\ 0 \\ 0 \end{bmatrix} v_d(k) + \begin{bmatrix} \mathbf{0}_{3\times1} \\ 0 \\ \mathbf{T}_1(1,1) \\ 0 \\ \mathbf{T}_3(1,1) \\ 0 \\ \mathbf{T}_5(1,1) \\ 0 \\ \mathbf{T}_7(1,1) \\ 0 \end{bmatrix} i_{\text{ref}}(k), \quad y(k) = \begin{bmatrix} \mathbf{C}_c & 0\ 0\ 0\ 0\ 0\ 0\ 0\ 0\ 0 \end{bmatrix} \begin{bmatrix} \mathbf{x}(k) \\ \phi(k) \\ \xi_1(k) \\ \xi_2(k) \\ \xi_3(k) \\ \xi_4(k) \\ \xi_5(k) \\ \xi_6(k) \\ \xi_7(k) \\ \xi_8(k) \end{bmatrix} \tag{21}$$

In a more compact form, (21) can be represented by

$$\boldsymbol{\rho}(k+1) = \boldsymbol{\mathcal{H}}\boldsymbol{\rho}(k) + \boldsymbol{\mathcal{H}_u}u(k) + \boldsymbol{\mathcal{H}}_d v_d(k) + \boldsymbol{\mathcal{H}}_r i_{\text{ref}}(k) \tag{22a}$$

$$y(k) = \boldsymbol{\mathcal{C}}\boldsymbol{\rho}(k) \tag{22b}$$

where $\boldsymbol{\rho} \in R^{12}$, $u \in R$, $y \in R$, $\boldsymbol{\mathcal{H}} \in R^{12\times12}$, $\boldsymbol{\mathcal{H}_u} \in R^{12\times1}$, $\boldsymbol{\mathcal{H}}_r \in R^{12\times1}$, $\boldsymbol{\mathcal{H}}_d \in R^{12\times1}$ and $\boldsymbol{\mathcal{C}} \in R^{1\times12}$.
This augmented model will be used to design the controller in the next section.

3 Model Predictive Control

For the system shown in Fig. 1, the control objective is to design a controller that ensures: (1) tracking of 60 Hz sinusoidal references; (2) disturbance rejection of grid voltages with frequencies of 60, 180, 300 and 420 Hz; (3) compliance with THD grid current limits presented in IEEE 1547 Standard; (4) robustness to grid uncertainties and variations. These objectives can be achieved with an MPC controller.

The traditional state-space MPC cost function usually takes into account only the future error and future control action (Camacho and Bordons 2004). However, in this particular problem, the energy of the resonant states must also be taken into account to avoid excessive values. Hence, the following cost function is used:

$$J = \sum_{i=1}^{N_y} \delta(y(k+i) - r(k+i))^2 + \sum_{j=1}^{4}\sum_{i=1}^{N_y} \delta_j \xi_{(2j-1)}(k+i)^2 + \sum_{i=0}^{N_u-1} \lambda u(k+i)^2 \tag{23}$$

where N_y, N_u, δ, δ_j, λ are, respectively, the prediction and control horizons, the weights of the future error, jth resonant state and future control action. One important aspect of this cost function is that only the output y has a reference, because the resonant states ξ_j are there to guarantee zero-error for these harmonics and do not have a specific desired reference.

It is possible to write (23) in matrix form, which makes it easier to organize the cost function. To do this, an auxiliary output and reference vectors are defined as:

$$\mathbf{y}'(k) = \begin{bmatrix} i_g(k) \\ \xi_1(k) \\ \xi_3(k) \\ \xi_5(k) \\ \xi_7(k) \end{bmatrix} = \mathbf{C}'\boldsymbol{\rho}(k) \tag{24}$$

where

$$\mathbf{C}' = \begin{bmatrix} 0\,0\,1\,0\,0\,0\,0\,0\,0\,0\,0\,0 \\ 0\,0\,0\,0\,1\,0\,0\,0\,0\,0\,0\,0 \\ 0\,0\,0\,0\,0\,0\,1\,0\,0\,0\,0\,0 \\ 0\,0\,0\,0\,0\,0\,0\,0\,1\,0\,0\,0 \\ 0\,0\,0\,0\,0\,0\,0\,0\,0\,0\,1\,0 \end{bmatrix},$$

and

$$\mathbf{r}'(k) = \begin{bmatrix} i_{\text{ref}}(k) \\ 0 \\ 0 \\ 0 \\ 0 \end{bmatrix} = \mathbb{I} i_{\text{ref}}(k), \quad \mathbb{I} = \begin{bmatrix} 1 \\ 0 \\ 0 \\ 0 \\ 0 \end{bmatrix}. \tag{25}$$

The following weight matrices are also necessary: $\mathbf{Q_y} = \text{diag}(\delta, \delta_1, \delta_2, \delta_3, \delta_4)$, where diag(.) defines a diagonal matrix whose elements are the parameters of the function. And $\mathbf{Q}'_\mathbf{y}$ is a block-diagonal matrix in which each element is $\mathbf{Q_y}$, $\mathbf{Q}'_\mathbf{y}$ has $5N_y$ elements:

$$\mathbf{Q}'_\mathbf{y} = \begin{bmatrix} \mathbf{Q_y} & 0 & 0 & 0 & 0 \\ 0 & \mathbf{Q_y} & 0 & 0 & 0 \\ 0 & 0 & \ddots & 0 & 0 \\ 0 & 0 & 0 & \mathbf{Q_y} & 0 \\ 0 & 0 & 0 & 0 & \mathbf{Q_y} \end{bmatrix}, \tag{26}$$

also, $\mathbf{Q}'_\mathbf{u} = \lambda \mathbf{I}_{N_u}$, where $\mathbf{I}_{N_u}$ is an identity square-matrix with dimension N_u. With these definitions, the cost function (23) can be written as:

$$J = (\mathbf{Y}' - \mathbf{W})^T \mathbf{Q}'_\mathbf{y} (\mathbf{Y}' - \mathbf{W}) + \mathbf{U} \mathbf{Q_u} \mathbf{U}, \tag{27}$$

with

$$\mathbf{Y}' = \begin{bmatrix} \mathbf{y}'(k+1) \\ \mathbf{y}'(k+2) \\ \vdots \\ \mathbf{y}'(k+N_y) \end{bmatrix}, \quad \mathbf{U}' = \begin{bmatrix} u(k) \\ u(k+1) \\ \vdots \\ u(k+N_u-1) \end{bmatrix}$$

$$\mathbf{W} = \begin{bmatrix} \mathbb{I} \\ \mathbb{I} \\ \vdots \\ \mathbb{I} \end{bmatrix} i_{\text{ref}}(k) = \mathbf{1} i_{\text{ref}}(k).$$

The vector $\mathbf{W}$ takes this simplified form because future references are unknown. It is worth noting that, usually, it is interesting to use future reference values in the MPC controller when they are available, which is generally the case for sinusoidal references. Since MPC uses the predicted future response of the system to compute the control action, if future references are taken into account, generally, the MPC is able to obtain a better control action that takes into account these future changes. However, in this particular application, the improvement was marginal; hence, a fixed reference was considered. This can be explained by the use of the resonant controllers. Since they already take into account a sinusoidal dynamic, future references are not necessary.

Now, the predictions vector $\mathbf{Y}'$ needs to be computed. From the auxiliary system equation (21), not considering $v_d(k)$ because it is not measurable, the prediction of the states at time $k+1$ based on the information on time k is

$$\boldsymbol{\rho}(k+1|k) = \boldsymbol{\mathcal{H}} \boldsymbol{\rho}(k) + \boldsymbol{\mathcal{H}_u} u(k) + \boldsymbol{\mathcal{H}}_r i_{\text{ref}}(k). \tag{28}$$

And the prediction at time $k+2$ given the information at time k is:

$$\boldsymbol{\rho}(k+2|k) = \boldsymbol{\mathcal{H}} \boldsymbol{\rho}(k+1|k) + \boldsymbol{\mathcal{H}_u} u(k+1) + \boldsymbol{\mathcal{H}}_r i_{\text{ref}}(k), \tag{29}$$

and notice that $i_{\text{ref}}(k)$ is used because $i_{\text{ref}}(k+1)$ is not known. Substituting (28) in (29):

$$\begin{aligned} \boldsymbol{\rho}(k+2|k) =& \boldsymbol{\mathcal{H}}^2 \boldsymbol{\rho}(k) + \boldsymbol{\mathcal{H}} \boldsymbol{\mathcal{H}_u} u(k) \\ &+ \boldsymbol{\mathcal{H}_u} u(k+1) + (\boldsymbol{\mathcal{H}} + \mathbf{I}) \boldsymbol{\mathcal{H}}_r i_{\text{ref}}(k). \end{aligned} \tag{30}$$

Following this pattern, the following can be derived:

$$\begin{aligned} \boldsymbol{\rho}(k+n|k) =& \boldsymbol{\mathcal{H}}^n \boldsymbol{\rho}(k) + \sum_{i=0}^{n-1} \boldsymbol{\mathcal{H}}^{n-1-i} \boldsymbol{\mathcal{H}_u} u(k+i) \\ &+ \left(\sum_{i=0}^{n-1} \boldsymbol{\mathcal{H}}^i \right) \boldsymbol{\mathcal{H}}_r i_{\text{ref}}(k). \end{aligned} \tag{31}$$

Considering (24), $\mathbf{Y}'$ can be written as

$$\mathbf{Y}' = \mathbf{G}\mathbf{U} + \mathbf{H}_{\boldsymbol{\rho}} \boldsymbol{\rho}(k) + \mathbf{H_r} i_{\text{ref}}(k) = \mathbf{G}\mathbf{U} + \mathbf{f}, \tag{32}$$

where $\mathbf{f}$ is the free response of the system, i.e., the response if the input becomes zero. Also, $\mathbf{G}$ is a block lower triangular matrix with its nonnull elements defined by $\mathbf{G_{ij}} = \mathbf{C}' \boldsymbol{\mathcal{H}}^{i-j} \boldsymbol{\mathcal{H}_u}$, and

$$\mathbf{H}_{\boldsymbol{\rho}} = \begin{bmatrix} \mathbf{C}' \boldsymbol{\mathcal{H}} \\ \mathbf{C}' \boldsymbol{\mathcal{H}}^{\mathbf{2}} \\ \vdots \\ \mathbf{C}' \boldsymbol{\mathcal{H}}^{\mathbf{N_y}} \end{bmatrix}, \quad \mathbf{H_r} = \begin{bmatrix} \mathbf{C}' \boldsymbol{\mathcal{H}}_\mathbf{r} \\ \mathbf{C}' (\boldsymbol{\mathcal{H}} + \mathbf{I}) \boldsymbol{\mathcal{H}}_r \\ \vdots \\ \mathbf{C}' \left(\sum_{i=0}^{N_y - 1} \boldsymbol{\mathcal{H}}^i \right) \boldsymbol{\mathcal{H}}_r \end{bmatrix}.$$

Using these definitions, the cost function (27) can be rearranged in the standard quadratic programming (QP) form:

$$J = \frac{1}{2} \mathbf{U}^T \mathbf{H} \mathbf{U} + \mathbf{b}^T \mathbf{U} + \mathbf{f_0}, \tag{33}$$

where

$$\begin{aligned} \mathbf{H} &= 2(\mathbf{G}^T \mathbf{Q}'_\mathbf{y} \mathbf{G} + \mathbf{Qu}), \\ \mathbf{b}^T &= 2(\mathbf{f} - \mathbf{1} i_{\text{ref}}(k))^T \mathbf{Q}'_\mathbf{y} \mathbf{G}, \end{aligned}$$

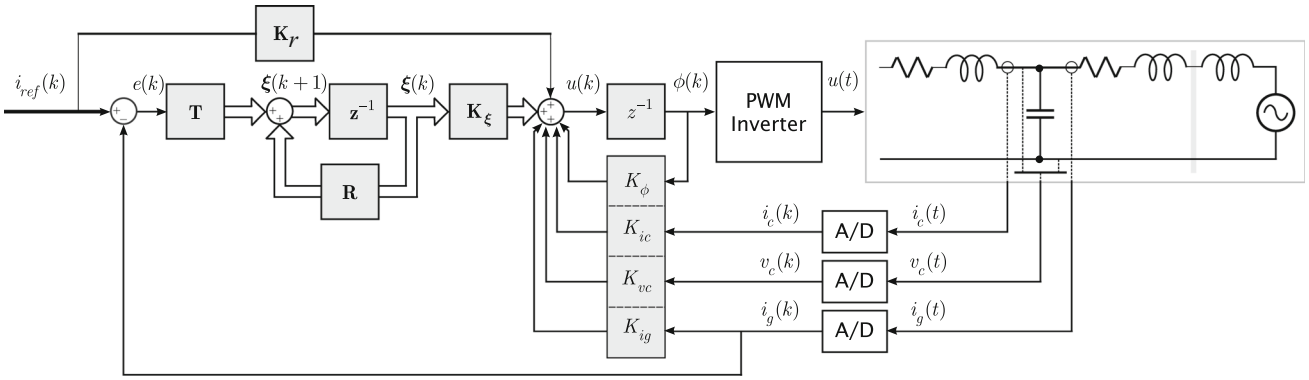

Fig. 2 Block diagram of the single-phase equivalent closed-loop system

$$\mathbf{f_0} = (\mathbf{f} - \mathbf{1}i_{\text{ref}}(k))^T \mathbf{Q}'_{\mathbf{y}}(\mathbf{f} - \mathbf{1}i_{\text{ref}}(k)).$$

If no constraints are considered in the optimization problem, the solution is given by

$$\mathbf{U} = \mathbf{K}(\mathbf{1}i_{\text{ref}}(k) - \mathbf{f}),$$

where $\mathbf{K} = (\mathbf{G}^T\mathbf{Q}'_{\mathbf{y}}\mathbf{G} + \mathbf{Q_u})^{-1}\mathbf{G}^T\mathbf{Q}'_{\mathbf{y}}$. Since only the first control input will be used, this last equation is reduced to:

$$u(k) = \mathbf{K_1}(\mathbf{1}i_{\text{ref}}(k) - \mathbf{f}), \tag{34}$$

where $\mathbf{K_1}$ is the first line of $\mathbf{K}$. In practice, this controller can be implemented as seen in Fig. 2. Where the gains can be obtained by rearranging (34)

$$u(k) = \mathbf{K_1}(\mathbf{1} - \mathbf{H_r})i_{\text{ref}}(k) - \mathbf{K_1}\mathbf{H}_{\boldsymbol{\rho}}\boldsymbol{\rho}(k) \tag{35}$$

$$= \mathbf{K_r}i_{\text{ref}}(k) + \mathbf{K}_{\boldsymbol{\rho}}\boldsymbol{\rho}(k), \tag{36}$$

where

$$\mathbf{K}_{\boldsymbol{\rho}} = -\mathbf{K_1}\mathbf{H}_{\boldsymbol{\rho}} = \left[K_{ic} \mid K_{vc} \mid K_{ig} \mid K_\phi \mid \mathbf{K}_\xi\right].$$

4 Robust Stability Analysis

An important feature of the proposed MPC design described in Sect. 3 is the fact that it leads to a linear controller with fixed gains. This approach allows the use of linear techniques to study the robustness of the closed-loop system such as LMI analysis.

Assuming the system (22) in closed-loop with the feedback control gains $\mathbf{K}_{\boldsymbol{\rho}}$ and the feed-forward gain $\mathbf{K_r}$, the resulting system can be described by

$$\begin{aligned}\boldsymbol{\rho}(k+1) &= \mathbf{A}_{cl}\boldsymbol{\rho}(k) + \mathbf{B}_{cl}i_{\text{ref}}(k) + \boldsymbol{\mathcal{H}}_d v_d(k)\\ y(k) &= \boldsymbol{\mathcal{C}}\boldsymbol{\rho}(k)\end{aligned} \tag{37a}$$

where $\mathbf{A}_{cl} = (\boldsymbol{\mathcal{H}} - \boldsymbol{\mathcal{H}}_{\boldsymbol{u}}\mathbf{K}_{\boldsymbol{\rho}})$ and $\mathbf{B}_{cl} = (\boldsymbol{\mathcal{H}}_{\boldsymbol{u}}\mathbf{K_r} + \boldsymbol{\mathcal{H}}_r)$

Now, consider the grid inductance L_{g2} as an uncertain parameter, possibly time variant, bounded between grid inductance limits. This type of uncertainty can be described by means of a polytopic model with two vertices. This closed-loop polytopic system is given by

$$\begin{aligned}\boldsymbol{\rho}(k+1) &= \mathbf{A}_{pp}(\mathbf{p}(k))\boldsymbol{\rho}(k)\\ &\quad + \mathbf{B}_{pp}(\mathbf{p}(k))i_{\text{ref}}(k) + \mathbf{B}_{dpp}(\mathbf{p}(k))v_d(k) \quad (38a)\\ y(k) &= \boldsymbol{\mathcal{C}}\boldsymbol{\rho}(k) \quad (38b)\end{aligned}$$

where

$$(\mathbf{A}_{pp}, \mathbf{B}_{pp}, \mathbf{B}_{dpp})(\mathbf{p}(k)) = \sum_{i=1}^{2} p_i(k)(\mathbf{A}_{pp}, \mathbf{B}_{pp}, \mathbf{B}_{dpp})_i,$$

$$\sum_{i=1}^{2} p_i = 1, \quad p_i \geq 0, \quad i = 1,\ 2 \tag{39}$$

where the vertices of (38) are obtained for the closed-loop system using the evaluation of the discrete augmented system (22) for the maximum and the minimum value of L_{g2} to be considered in the analysis.

To ensure robustness for all values of the given uncertainty interval, Theorem 1 must be satisfied.

Theorem 1 *If symmetric positive definite matrices $\boldsymbol{\mathcal{S}}_i \in \mathbb{R}^{2n+4\times 2n+4}$, $i = 1, 2$, being n the number of resonant controllers, and $\boldsymbol{\mathcal{G}} \in \mathbb{R}^{2n+4\times 2n+4}$ exist such that*

$$\begin{bmatrix} \boldsymbol{\mathcal{G}} + \boldsymbol{\mathcal{G}}' - \boldsymbol{\mathcal{S}}_i & \boldsymbol{\mathcal{G}}'\mathbf{A}'_{pp\,j} \\ \mathbf{A}_{pp\,j}\boldsymbol{\mathcal{G}} & \boldsymbol{\mathcal{S}}_j \end{bmatrix} > \mathbf{0},\ i = 1, 2,\ j = 1, 2 \tag{40}$$

then the following closed-loop properties are guaranteed:

(i) *Closed-loop robust stability even for arbitrarily fast variations of L_g;*
(ii) *That the eigenvalues of $\mathbf{A}_{pp}(p(k))$ belong to the unit circle;*

The proof of Theorem 1 can be found in Daafouz and Bernussou (2001).

5 Simulation and Experimental Results

Considering a grid-connected inverter as shown in Fig. 1, with parameters given in Table 1, the MPC controller is designed to guarantee tracking of 60 Hz sinusoidal references and disturbance rejection of grid voltage harmonics in third, fifth and seventh fundamental harmonics considering the nominal inductance value of the grid. To achieve this specification, four resonant controllers were used at 60, 180, 300 and 420 Hz, with a common damping factor of $\zeta = 0.00001$.

Since the MPC has many tuning parameters, a study was made to find the best controller configuration considering the plant described earlier. In this study, three different performance indexes were used: integral of squared error (ISE), integral of squared derivative (ISD), and integral of time squared error (ITSE). The equations for each one are given below:

$$\text{ISE} = \int_0^\infty e(t)^2 \mathrm{d}t \tag{41}$$

$$\text{ISD} = \int_0^\infty \dot{y}^2 \mathrm{d}t \tag{42}$$

$$\text{ITSE} = \int_0^\infty t e(t)^2 \mathrm{d}t \tag{43}$$

The ISE index is straightforward and relates to how well the control system tracks the reference signal. The ISD measures the oscillations present in the closed-loop system, thus complementing the ISE index. This index is important because it is possible for the controller to have fast tracking capabilities with excessive oscillations, which is undesirable, and this behavior is not reflected in the ISE index. Lastly, the ITSE index helps to detect whether the system is taking too long to track the reference.

Table 1 System parameters

System description		
Nominal values	Power	5.4 kW
	Grid phase voltage	220 Vrms
	Grid phase current	14.14 Arms
	Grid frequency	60 Hz
	Switching frequency	10020 Hz
	Sampling period	1/20040 s
	V_{cc}	420 V
LCL filter	L_{c1}	1 mH
	L_{g1}	0.3 mH
	C_f	62 μF
Nominal grid inductance	L_{g2}	0 mH

In the tuning study, the controller parameters were varied and then the indexes were computed for a fixed simulation scenario. There are basically two groups of parameters: cost function weights and horizons. For each group, a set of 25 simulations were made.

For the first group, the future error weight δ and resonant states δ_j were varied and the control weight remained constant ($\lambda = 1$). Since there is only one manipulated variable, and the weights are relative in regard to each other, i.e., if you multiply every weight by a constant factor the optimal solution does not change, it is easier to maintain this particular weight fixed. Also, all δ_j have the same value for each simulation. In this simulation set, the control and prediction horizon are constant and the weights are varied in the range [0.4, 20]. The results are presented in Fig. 3, where each plot shows the results for different indexes.

From what can be seen in Fig. 3, there is a clear optimal region that minimizes the three indexes, which is around $\delta = 20$ and $\delta_j = 1$. One important characteristic to notice is that if the resonant weights are greater than the future error weight, there is a clear rise in the values of the indexes, i.e., the closed-loop response deteriorates dramatically. This behavior makes sense, because if the resonant weights are relatively higher than the error one, this means that the minimization procedure will try to minimize the values of the resonant signals; however, these signals are essential for the controller to track the reference appropriately and hence the worst closed-loop response.

For the second group of parameters, the horizons, the weights were maintained constant and the control and prediction horizons were varied from 1 to 333 and from 20 to 500, respectively. It is important to remember that it does not make sense for the control horizon to be bigger than the prediction horizon; hence, only the appropriate combinations were tested. The results are shown in Fig. 4 where there is a clear region around $N_y = 100$ and $N_u = 20$ where the indexes are lower.

Hence, based on these results, the following tuning parameters were used for the MPC controller design:

- Prediction horizon $N_y = 100$: considering that the sampling frequency is 20040 (Hz), the horizon is of 0.005 (s) in the future, approximately a third of a 60 Hz cycle;
- Control horizon of $N_u = 20$;
- Control weight $\lambda = 1$;
- States weight $\delta_j = 1$, $j = 1, \ldots, 4$;
- Error weight $\delta = 20$: this was chosen higher than the states weight so that the error has a larger influence in the computation of the control action.

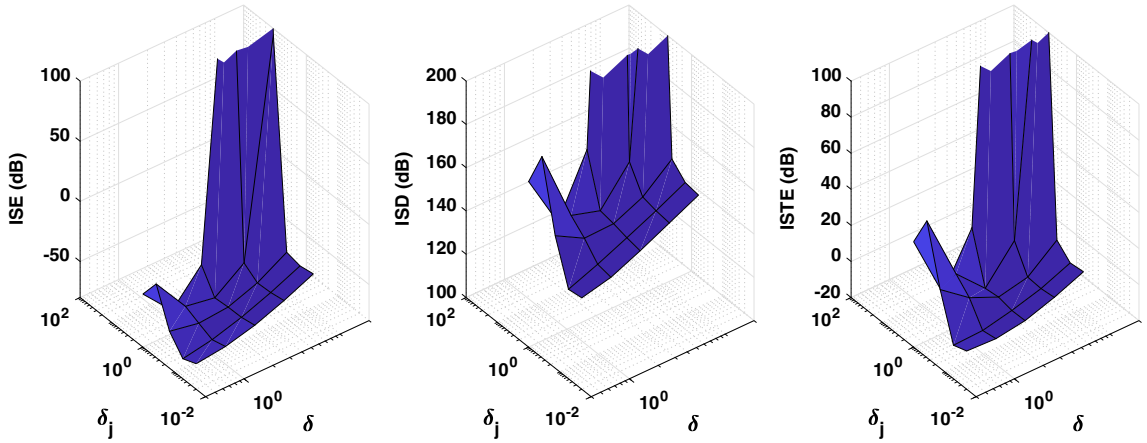

Fig. 3 Performance indexes for varying weights

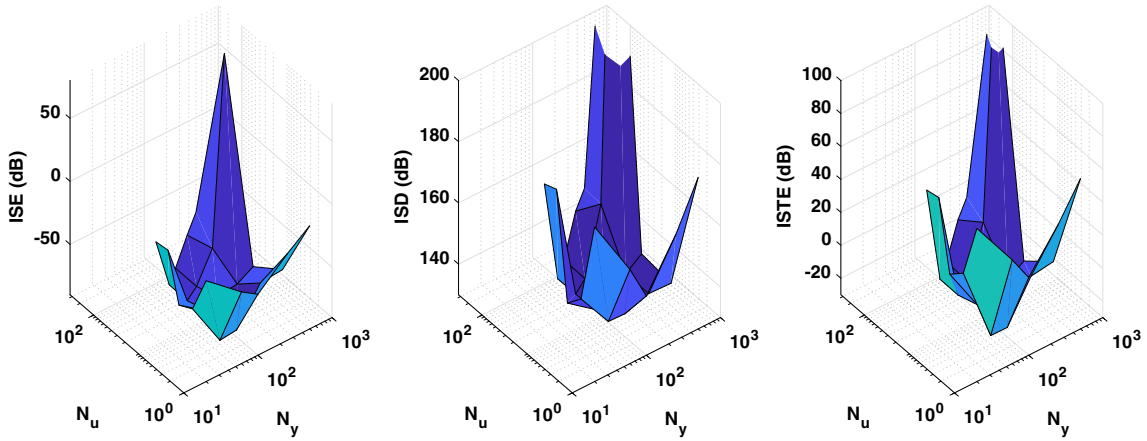

Fig. 4 Performance indexes for varying horizons

Following the steps in Sect. 3 and the block diagram in Fig. 2 with the parameters presented in Table 1, the controller gains, in the unconstrained case, are:

$$\mathbf{K_r} = \begin{bmatrix} 5.015699806 \end{bmatrix} \tag{44}$$

$$\mathbf{K_x} = \begin{bmatrix} -6.015976889 \\ -0.536366141 \\ 1.000277083 \end{bmatrix}^T = \begin{bmatrix} K_{ic} \\ K_{vc} \\ K_{ig} \end{bmatrix}^T \tag{45}$$

$$\mathbf{K}_\phi = \begin{bmatrix} -0.286145288 \end{bmatrix} \tag{46}$$

$$\mathbf{K}_\xi = \begin{bmatrix} 24.81382376 \\ -24.40335775 \\ 9.234246863 \\ -9.039906238 \\ 4.265396784 \\ -4.368170789 \\ 1.655606318 \\ -1.817369436 \end{bmatrix}^T \tag{47}$$

To ensure the robustness of the closed-loop system, an LMI analysis was performed using Theorem 1. The control gains (44), (45), (46), (47), are used to evaluate the polytopic model (38). The optimization problem was solved using the Robust Control Toolbox from MATLAB. The controller gains satisfied Theorem 1, ensuring robust stability against grid inductance uncertainties and arbitrarily fast variations inside the inductance limits used in the analysis ($Lg_2 \in [0, \quad 1]$ mH).

5.1 Closed-loop Frequency-Domain Analysis

The closed-loop frequency responses of the reference i_{ref} to the output current i_g for different values of L_{g2} in the uncertainty interval are shown in Fig. 5. The frequency responses were carried out using increments of 0.1 mH in the specified interval, and the nominal frequency response was highlighted with a different color. The same analysis was performed to obtain the frequency responses of the voltage disturbance v_d to the output current i_g. The results are shown in Fig. 6.

Notice that in Fig. 5 the frequency response has 0 dB gain and a phase of 0 degrees at 60 Hz for all tested values of L_{g2}, and this result certifies the reference tracking capabilities of

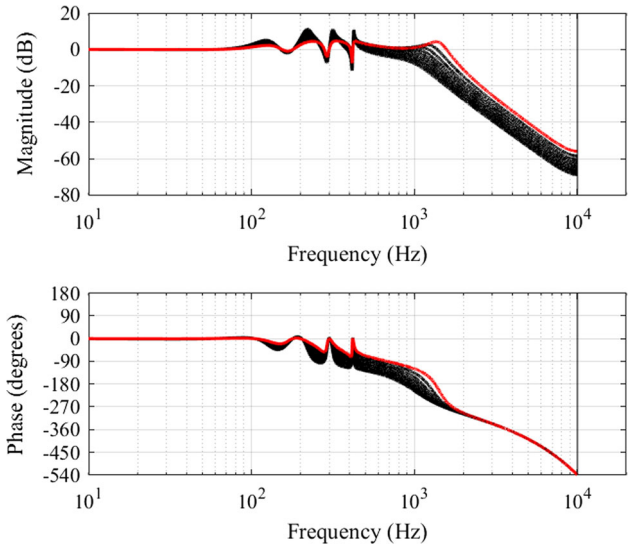

Fig. 5 Bode diagram from the current reference i_{ref} to the system output (i_g)

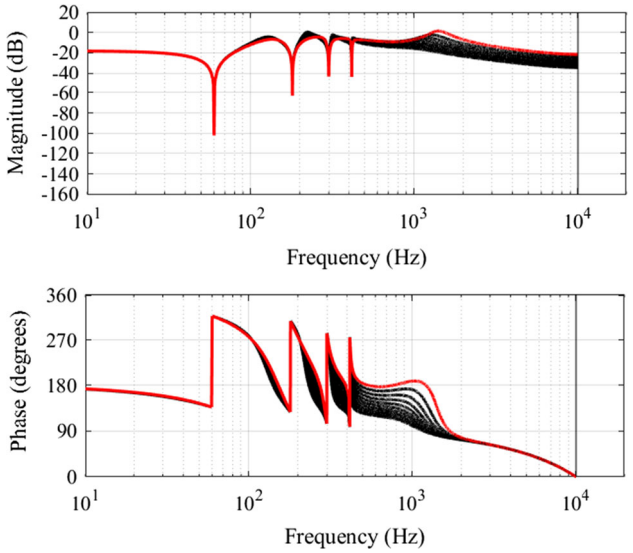

Fig. 6 Bode diagram from the voltage disturbance v_d to the system output (i_g)

the MPC controller for all inductance values in the uncertainty interval. In Fig. 6, note the very low magnitude gains for the frequencies specified for the resonant controllers. This low-gain behavior ensures the disturbance rejection at the first, third, fifth and seventh harmonics of the grid voltage for all values of L_{g2} included in uncertainty interval.

5.2 Simulation Results

To study the transient responses of the closed-loop system, the MPC controller was tested for the minimum (nominal) and the maximum values of the grid inductance. The tests

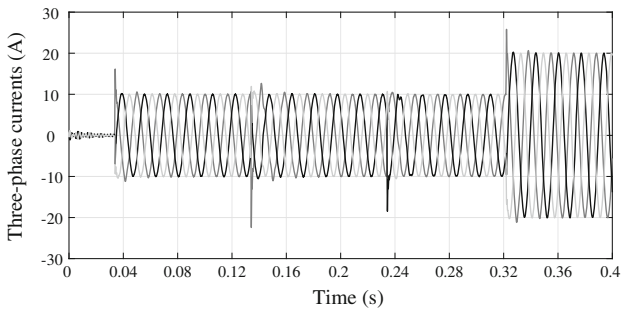

Fig. 7 Simulation results: three-phase grid currents for minimum L_{g2} (0 mH)

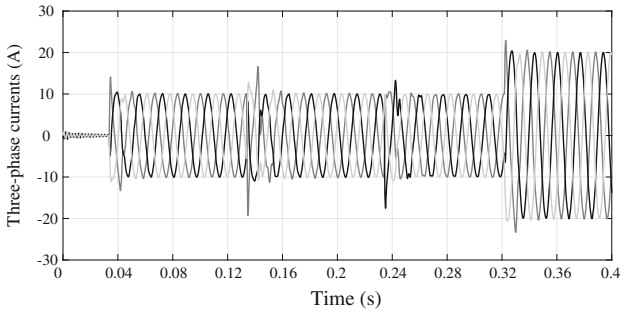

Fig. 8 Simulation results: three-phase grid currents for maximum L_{g2} (1 mH)

were implemented using PSIM software and space vector modulation (POWERSIM 2011). To assess the reference tracking capabilities, α and β references were varied, with fast amplitude and phase variations representing different conditions of active and reactive power injected in the grid. The reference for the α current is given by

$$
\begin{aligned}
&t \in [0, 2T_g) && i_{\text{ref}}(t) = 0;\\
&t \in [2T_g, 8T_g) && i_{\text{ref}}(t) = 10\cos(2\pi 60t + \pi/2);\\
&t \in [8T_g, 14T_g) && i_{\text{ref}}(t) = -10\cos(2\pi 60t + \pi/2);\\
&t \in [14T_g, 20T_g) && i_{\text{ref}}(t) = 10\cos(2\pi 60t);\\
&t \in [20T_g, 24T_g] && i_{\text{ref}}(t) = 20\cos(2\pi 60t).
\end{aligned}
$$

where $T_g = 1/60\,\text{s}$. The reference for the β current has the same pattern, but a phase of $\pi/2$ radians is added to the signals.

The result for the minimum value of the grid inductance is presented in Fig. 7, and the result for the maximum value is shown in Fig. 8. One can see that for both values of the impedance the controller can cope with the reference variations with fast settling times. The overshoot presented in the simulations are inside the expected range and did not bring any problem for the system.

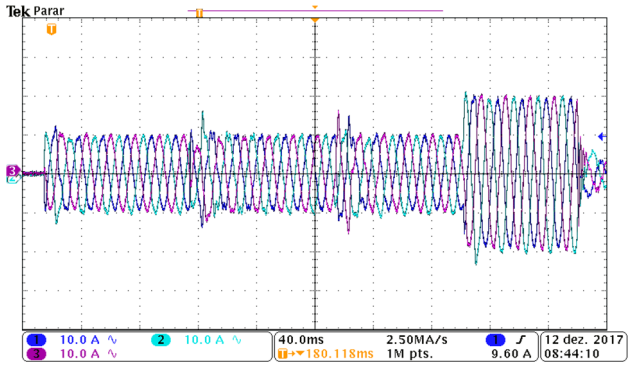

Fig. 9 Experimental result: grid currents injected to the grid

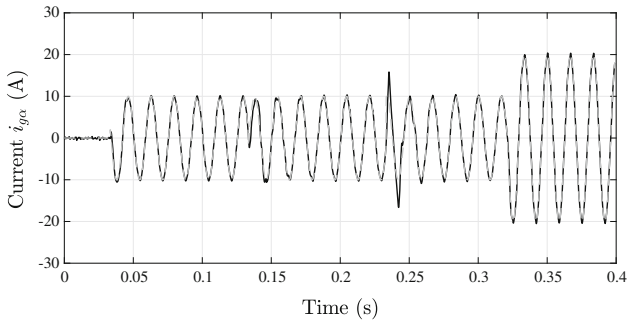

Fig. 10 Experimental result: reference tracking for α coordinates, $i_{ref\alpha}$ represented by the dashed line

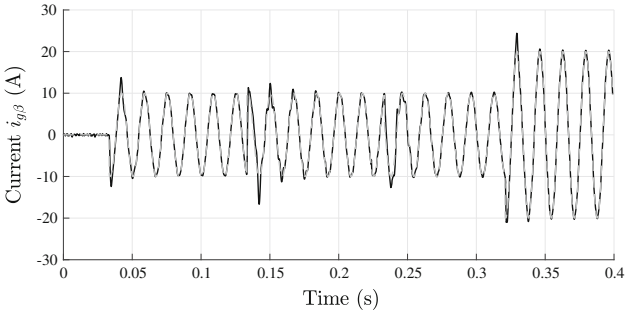

Fig. 11 Experimental result: reference tracking for β coordinates, $i_{ref\beta}$ represented by the dashed line

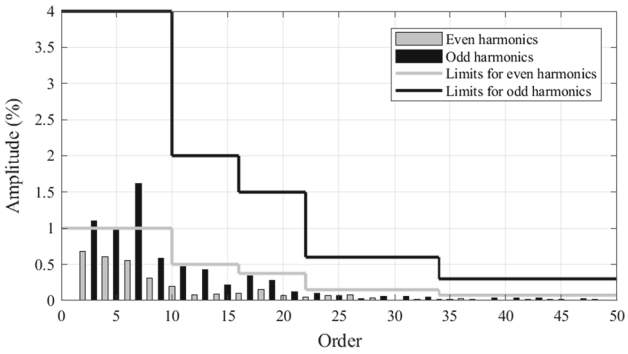

Fig. 12 Harmonic content of phase a current and IEEE 1547 Standard harmonic limits

5.3 Experimental Results

In order to have an experimental validation of the simulation results the tests were repeated in practice. The controller was implemented using a 32-bit floating-point DSP TMS320F28335 from Texas Instruments. The experimental results for the same reference pattern used in Figs. 7 and 8 are presented in Fig. 9, in which one can see the fast settling times of the grid currents injected in the grid.

It is important to notice that in the experimental results the grid inductance was uncertain once the inverter was connected into a real grid.

To illustrate the good tracking capabilities, Figs. 10 and 11 show the α and β coordinates references and their respective output grid currents. In these figures, one can see the fast transient responses with low current peaks which are suitable for the application.

To verify whether the grid currents comply with IEEE 1547 Standard, the harmonic content using 12 cycles in sinusoidal steady state with nominal values for the grid voltage and impedance was studied. Figure 12 presents the harmonic content for the grid current only for phase a. This pattern is similar for other phases. The THD obtained was 2.7168 %, and the harmonic limits presented in IEEE 1547 were not violated.

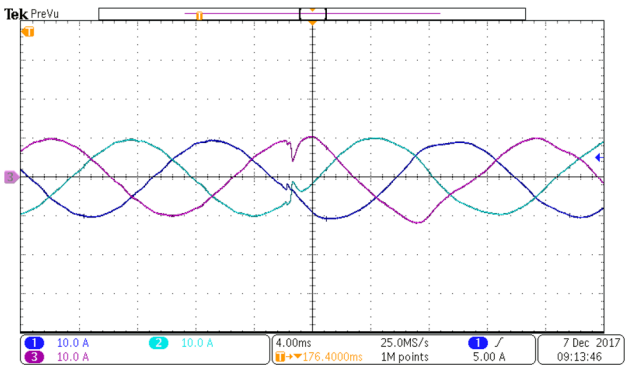

Fig. 13 Experimental result: three-phase grid currents in the presence of a variation of L_{g2} from 0 mH to 1 mH

Finally, to confirm the results obtained for the LMI analysis, a test of parameter variation was carried out. For this test, the system was disconnected from grid ($v_d = 0$ V) and then the grid inductances (L_{g2}) were switched from 0 mH to 1 mH. The result is shown in Fig. 13, where it can be seen that the system remains stable confirming the robustness certified theoretically by the factibility of Theorem 1.

6 Conclusion

This work presented a CCS-MPC controller applied to a three-phase grid-connected inverter. The main control objectives are to track sinusoidal current references, to reject harmonic disturbances, and to obtain a closed-loop that is robust in regard to uncertainties and variations of the grid inductance. To do this, an augmented state-space model of the process was used that included the harmonic characteristics of importance to the problem. Then, the traditional unconstrained CCS-MPC approach was used to derive the controller. An interesting point is that this augmented model can easily be adapted to include other harmonics.

The resulting controller has fixed gains and was implemented using a structure similar to the traditional state-feedback control law. To show that the resulting controller is robust in regard to the specified parametric uncertainties and variations, an *a posteriori* LMI approach was proposed. Simulation and experimental results were provided which confirmed that all control objectives were satisfied. Also, the harmonic content of the results were studied, and they were all within the limits specified in the IEEE 1547 Standard.

With these results, the authors believe that the proposed approach can be used as an alternative to classical controllers in this particular application. And, the methodology is general enough that it can be easily applied to other systems for which state-feedback control laws lead to suitable results. In relations to the classical controllers, the following remarks are important about the proposed approach:

- Since the *dq*-transform is not necessary, this approach avoid the limitations of the SRFPI: (i) coupled dynamics of the *d* and *q* coordinates of the LCL filter, which impacts the transient response; (i) use of multiple reference frames, which makes the controller more complex.
- In relation to the FCS-MPC, it has a fixed switching frequency and results in a linear controller, which enables the use of linear analysis technique to, as explained earlier, prove robustness and verify closed-loop properties in the frequency domain.
- Contrary to the LQR method, the CCS-MPC does not guarantee nominal closed-loop stability. However, the proposed approach uses an *a posteriori* LMI analysis of the system to prove nominal stability and robustness against uncertain and possibly time-varying parameters.

As a future work, the constrained CCS-MPC will be considered. There are always limitations in the system such as saturations, or rate limitation, that should be considered in the computation of the control signal. However, in these cases the optimization problem of MPC does not have a algebraic solution, making the use of iterative optimization algorithms a necessity. These algorithms can take some time to reach a solution that might not be within the relatively small sampling time. Hence, a research will be made to verify whether there are simplified algorithms that can be embedded in a DSP and can cope with this limitation.

Acknowledgements This study was financed in part by the Coordenação de Aperfeiçoamento de Pessoal de Nível Superior - Brasil (CAPES/PROEX) - Finance Code 001. The authors would also like to thank the INCT-GD and the finance agencies (CNPq 465640/2014-1, CNPq 309536/2018-9, CAPES 23038.000776/2017-54, FAPERGS 17/2551-0000517-1).

References

Bianchi, F. D., Egea-Alvarez, A., Junyent-Ferré, A., & Gomis-Bellmunt, O. (2012). Optimal control of voltage source converters under power system faults. *Control Engineering Practice*, *20*(5), 539–546.

Busada, C. A., Jorge, S. G., & Solsona, J. A. (2015). Full-state feedback equivalent controller for active damping in LCL-filtered grid-connected inverters using a reduced number of sensors. *IEEE Transactions on Industrial Electronics*, *62*(10), 5993–6002. https://doi.org/10.1109/TIE.2015.2424391.

Camacho, E., & Bordons, C. (2004). *Model predictive control*. Berlin: Springer.

Cardoso, R., de Camargo, R. F., Pinheiro, H., & Gründling, H. A. (2008). Kalman filter based synchronisation methods. *IET Generation Transmission Distribution*, *2*(4), 542–555.

Daafouz, J., & Bernussou, J. (2001). Parameter dependent Lyapunov functions for discrete time systems with time varying parameter uncertainties. *Systems & Control Letters*, *43*(5), 355–359.

Duesterhoeft, W., Schulz, M. W., & Clarke, E. (1951). Determination of instantaneous currents and voltages by means of alpha, beta, and zero components. *Transactions of the American Institute of Electrical Engineers*, *70*(2), 1248–1255. https://doi.org/10.1109/T-AIEE.1951.5060554.

Falkowski, P., & Sikorski, A. (2018a). Comparative analysis of finite control set model predictive control methods for grid-connected AC-DC converters with LCL filter. In Proceedings of IEEE 27th international symposium industrial electronics (ISIE), pp. 193–200. https://doi.org/10.1109/ISIE.2018.8433673

Falkowski, P., & Sikorski, A. (2018b). Finite control set model predictive control for grid-connected AC–DC converters with LCL filter. *IEEE Transactions on Industrial Electronics*, *65*(4), 2844–2852. https://doi.org/10.1109/TIE.2017.2750627.

Ferreira, S. C., Gonzatti, R. B., Pereira, R. R., da Silva, C. H., da Silva, L. B., & Lambert-Torres, G. (2018). Finite control set model predictive control for dynamic reactive power compensation with hybrid active power filters. *IEEE Transactions on Industrial Electronics*, *65*(3), 2608–2617.

Francis, B. A., & Wonham, W. M. (1976). The internal model principle of control theory. *Automatica*, *12*(5), 457–465.

Huerta, F., Pizarro, D., Cobreces, S., Rodriguez, F., Giron, C., & Rodriguez, A. (2012). LQG servo controller for the current control of LCL grid-connected voltage-source converters. *IEEE Transactions on Industrial Electronics*, *59*(11), 4272–4284. https://doi.org/10.1109/TIE.2011.2179273.

IEC: IEC 61000-3-2—electromagnetic compatibility (emc)-part 3–2: Limits–limits for harmonic currents emission (equipment input ≤ 16 a per phase) (2018).

IEC: IEC 61727 Photovoltaic (PV) Systems—Characteristics of the Utility Interface (2004).

IEEE: IEEE:1547 standard for interconnecting distributed resources with electric power systems (2011).

Koch, G. G., Maccari, L. A., Oliveira, R. C. L. F., & Montagner, V. F. (2019). Robust $\mathcal{H}_\infty$ state feedback controllers based on linear matrix inequalities applied to grid-connected converters. *IEEE Transactions on Industrial Electronics*, *66*(8), 6021–6031. https://doi.org/10.1109/TIE.2018.2870406.

Kouro, S., Cortes, P., Vargas, R., Ammann, U., & Rodriguez, J. (2009). Model predictive control—a simple and powerful method to control power converters. *IEEE Transactions on Industrial Electronics*, *56*(6), 1826–1838. https://doi.org/10.1109/TIE.2008.2008349.

Kukkola, J., & Hinkkanen, M. (2013). Observer-based state-space current control for a three-phase grid-connected converter equipped with an LCL filter. pp. 1371–1378. https://doi.org/10.1109/ECCE.2013.6646865.

Lekouaghet, B., Boukabou, A., Lourci, N., & Bedrine, K. (2018). Control of PV grid connected systems using mpc technique and different inverter configuration models. *Electric Power Systems Research*, *154*, 287–298.

Liserre, M., Teodorescu, R., & Blaabjerg, F. (2006). Multiple harmonics control for three-phase grid converter systems with the use of PI-RES current controller in a rotating frame. *IEEE Transactions on Power Electronics*, *21*(3), 836–841. https://doi.org/10.1109/TPEL.2006.875566.

Maccari, L., Do Amaral Santini, C., Pinheiro, H., de Oliveira, R., & Foletto Montagner, V. (2015). Robust optimal current control for grid-connected three-phase pulse-width modulated converters. *IET Power Electronics*, *8*(8), 1490–1499. https://doi.org/10.1049/iet-pel.2014.0787.

Maccari, L.A., Montagner, V.F., & Lima, D.M. (2016). Model predictive current controller applied to grid-connected LCL filters. In Proceedings of 2016 12th IEEE international conference on industry applications (INDUSCON), pp. 1–6. https://doi.org/10.1109/INDUSCON.2016.7874478.

Maccari, L. A., Pinheiro, H., Oliveira, R. C., & e Vinícius, F. (2017). Montagner Robust pole location with experimental validation for three-phase grid-connected converters. *Control Engineering Practice*, *59*(Supplement C), 16–26. https://doi.org/10.1016/j.conengprac.2016.10.013.

Maccari, L. A, Jr., Massing, J. R., Schuch, L., Rech, C., Pinheiro, H., Oliveira, R. C. L. F., et al. (2014). LMI-based control for grid-connected converters with LCL filters under uncertain parameters. *IEEE Transactions on Power Electronics*, *29*(7), 3776–3785. https://doi.org/10.1109/TPEL.2013.2279015.

Nauman, M., & Hasan, A. (2016). Efficient implicit model-predictive control of a three-phase inverter with an output LC filter. *IEEE Transactions on Power Electronics*, *31*(9), 6075–6078. https://doi.org/10.1109/TPEL.2016.2535263.

Panten, N., Hoffmann, N., & Fuchs, F. W. (2016). Finite control set model predictive current control for grid-connected voltage-source converters with LCL filters: A study based on different state feedbacks. *IEEE Transactions on Power Electronics*, *31*(7), 5189–5200. https://doi.org/10.1109/TPEL.2015.2478862.

Peña-Alzola, R., Liserre, M., Blaabjerg, F., Sebastián, R., Dannehl, J., & Fuchs, F. W. (2013). Analysis of the passive damping losses in LCL-filter-based grid converters. *IEEE Transactions on Power Electronics*, *28*(6), 2642–2646. https://doi.org/10.1109/TPEL.2012.2222931.

POWERSIM: PSIM User's guide version 9.1. (2011).

Qin, S. J., & Badgwell, T. A. (2003). A survey of industrial model predictive control technology. *Control Engineering Practice*, *11*(7), 733–764.

Rodriguez, J., Kazmierkowski, M. P., Espinoza, J. R., Zanchetta, P., Abu-Rub, H., Young, H. A., et al. (2013). State of the art of finite control set model predictive control in power electronics. *IEEE Transactions on Industrial Informatics*, *9*(2), 1003–1016. https://doi.org/10.1109/TII.2012.2221469.

Safonov, M., & Athans, M. (1977). Gain and phase margin for multiloop LQG regulators. *IEEE Transactions on Automatic Control*, *22*(2), 173–179. https://doi.org/10.1109/TAC.1977.1101470.

Sultana, W. R., Sahoo, S. K., Sukchai, S., Yamuna, S., & Venkatesh, D. (2017). A review on state of art development of model predictive control for renewable energy applications. *Renewable and Sustainable Energy Reviews*, *76*, 391–406. https://doi.org/10.1016/j.rser.2017.03.058.

Teodorescu, R., Liserre, M., & Rodríguez, P. (2011). *Grid converters for photovoltaic and wind power systems*. Hoboken: Wiley.

Twining, E., & Holmes, D. (2003). Grid current regulation of a three-phase voltage source inverter with an LCL input filter. *IEEE Transactions on Power Electronics*, *18*(3), 888–895. https://doi.org/10.1109/TPEL.2003.810838.

Umbrí, F., Gordillo, F., Gómez-Estern, F., Salas, F., Portillo, R. C., & Vázquez, S. (2014). Voltage balancing in three-level neutral-point-clamped converters via Luenberger observer. *Control Engineering Practice*, *25*, 36–44.

Vazquez, S., Rodriguez, J., Rivera, M., Franquelo, L. G., & Norambuena, M. (2017). Model predictive control for power converters and drives: Advances and trends. *IEEE Transactions on Industrial Electronics*, *64*(2), 935–947. https://doi.org/10.1109/TIE.2016.2625238.

Wu, E., & Lehn, P. (2006). Digital current control of a voltage source converter with active damping of LCL resonance. *IEEE Transactions on Power Electronics*, *21*(5), 1364–1373. https://doi.org/10.1109/TPEL.2006.880271.

Young, H. A., Perez, M. A., & Rodriguez, J. (2016). Analysis of finite-control-set model predictive current control with model parameter mismatch in a three-phase inverter. *IEEE Transactions on Industrial Electronics*, *63*(5), 3100–3107. https://doi.org/10.1109/TIE.2016.2515072.

Zmood, D. N., & Holmes, D. G. (2003). Stationary frame current regulation of PWM inverters with zero steady-state error. *IEEE Transactions on Power Electronics*, *18*(3), 814–822. https://doi.org/10.1109/TPEL.2003.810852.